Applied Catalysis B: Environmental 236 (2018) 1–12

Contents lists available at ScienceDirect

Applied Catalysis B: Environmental

journal homepage: www.elsevier.com/locate/apcatb

Hydrodeoxygenation of pinyon-juniper catalytic pyrolysis oil using red mud-supported nickel catalysts

Hossein Jahromi*, Foster A. Agblevor

USTAR Bioenergy Center, Department of Biological Engineering, Utah State University, UT 84322, USA

ARTICLE INFO

Keywords:
Red mud
Hydrodeoxygenation
Nickel catalyst
Pyrolysis oil
Pinyon-juniper

ABSTRACT

Red mud (RM) is an alkaline waste generated in the Bayer process of alumina production. In the present study red mud supported nickel catalysts (Ni/RM) were prepared at different concentrations of nickel (10, 20, 30, 40, 50, and 65 wt.%) and used to hydrodeoxygenate (HDO) pinyon-juniper (PJ) catalytic pyrolysis oil. Increasing the nickel content improved the activity of Ni/RM catalysts for HDO reactions. Maximum organic liquid yield (68.6%) was obtained when 40%Ni/RM was used. The upgraded oil had oxygen content of 1.35 wt.% and higher heating value of 45.77 MJ/kg compared to 24.88 wt.% and 28.41 MJ/kg, respectively, for the crude oil. For comparison, commercial Ni/SiO_2-Al_2O_3 was also evaluated in HDO experiments. The HDO oil properties obtained using 40%Ni/RM at reaction temperature of 400 °C was similar to that of commercial Ni/SiO_2-Al_2O_3 at reaction temperature of 450 °C. However, the organic liquid yield was much higher for 40%Ni/RM (68.6%) compared to the commercial Ni/SiO_2-Al_2O_3 (41.8%). The commercial Ni/SiO_2-Al_2O_3 produced more gas (27.6%) than the 40%Ni/RM (16.4%) and the coke yields for the commercial catalyst and Ni/RM catalyst were 7.3% and 4.2% respectively. Overall, application of Ni/RM improved HDO reactions and reduced cracking and coke formation compared to commercial Ni/SiO_2-Al_2O_3.

1. Introduction

The world's energy consumption is increasing due to population growth and economic developments. Fossil fuels consumption has increased significantly since the industrial revolution and constitutes more than 80% of the world primary energy consumption is derived from fossil fuels [1]. This excessive dependence on fossil fuels contributes to severe environmental degradation such as water, air and soil pollutions. Biomass provides a promising feedstock for producing renewable fuels and chemicals, especially liquid fuels [2–4]. A potentially efficient and cost-effective method for converting biomass to liquid fuel (bio-oil) is through fast pyrolysis. This method requires low capital investment and can be easily applied in commercial plants [5–7]. Fast pyrolysis is a thermochemical process that decomposes biomass components of cellulose, hemicellulose and lignin into bio-oil, bio-char, and gas [8,9]. Pyrolysis oil has acidic and corrosive properties, high water content, and a relatively low energy density as compared to conventional petroleum-derived fuels, making it unusable as transportation fuels [10,11]. Consequently, bio-oil upgrading is needed to reduce its water and oxygen contents [12].

Hydrodeoxygenation (HDO), which is considered an effective method for bio-oil upgrading, involves the stabilization and selective removal of oxygen from untreated bio-oil through its catalytic reaction with hydrogen [10,13]. Catalysts play a critical role in bio-oil HDO, and many catalysts have been investigated [14]. Several categories of catalysts including noble metal and sulfided metal catalysts have been investigated [15,16]. Noble metal catalysts such as Ru/C, Ru/TiO_2, Ru/Al_2O_3, Pt/C, and Pd/C were used for HDO of bio-oil [17,18]. The results showed that Ru/C catalyst was superior to typical HDO catalysts such as sulfided NiMo/Al_2O_3 and CoMo/Al_2O_3 for bio-oil upgrading [17]. However, the noble metal catalysts have limitations which include high cost and limited supply. The sulfided catalysts are less suitable for bio-oil HDO due to the economic factors of using sulfur, product contamination, and the poor stability of alumina support (deactivation by water) [19]. Non-noble metal catalysts such as metallic Ni, Cu, Fe or their bimetallic combination supported on Al_2O_3 were also investigated, and they were shown to be very active in bio-oil HDO [20]. However, the problem of alumina's poor tolerance of water still existed in these tests, which can easily cause catalyst deactivation [21]. Therefore, development of an effective, readily available catalyst support can play a crucial role in HDO process both technically and economically.

Developing catalysts from waste materials is an effective means of value addition to the waste. Red mud has received considerable

* Corresponding author.
E-mail address: hossein.jahromi@aggiemail.usu.edu (H. Jahromi).

https://doi.org/10.1016/j.apcatb.2018.05.008
Received 26 December 2017; Received in revised form 1 May 2018; Accepted 3 May 2018
Available online 04 May 2018
0926-3373/

attention in this regard. Red mud (RM) or red sludge is a caustic waste material generated during the Bayer process for alumina production [22]. There are many problems with managing RM slurry. Some of these problems are costly maintenance of RM pond areas, risk of caustic pollutants for all living organisms, leakage of alkaline contaminants into groundwater resources, and overflow of materials during rainy seasons that can cause harmful effects on surrounding environment [22,23]. RM consists of compounds originally present in the parent mineral and those introduced during the Bayer process. The main chemical components of RM are Fe_2O_3, Al_2O_3, SiO_2, CaO, Na_2O, TiO, K_2O and MgO and a number of minor constituents such as Cr, V, S, Ni, Cu, Mn, Zn etc [23].

RM has been investigated as catalyst for various applications, including pyrolysis of biomass [24,25], hydrogenation and liquefaction [26–31], hydrodechlorination and desulfurization reactions [32–34], and exhaust gas clean-up [35,36]. RM has also been used as catalyst in other reactions such as degradation of polyvinyl chloride containing polymer mixtures into fuel oil [37,38], conversion of waste oil and waste plastic to fuel [39], heavy crude oil hydrotreating [40], ammonia decomposition in presence of sulfur compounds [41], and nitrile synthesis from aldehydes and hydroxylamine [42]. Furthermore, RM has recently been used as catalyst for removal of organics from water [43,44], biodiesel production [45], and methanogenesis reaction [46]. The conversion of RM into a value added product such as heterogeneous catalyst can be considered a promising technology for the final destination of the residue.

The main objective of this work is to investigate the application of RM-supported nickel catalysts (Ni/RM) for upgrading of pyrolysis oil (bio-oil) via hydrodeoxygenation. Our previous study showed that Ni/RM can be used as an effective catalyst for the hydrodeoxygenation of guaiacol as a bio-oil model compound [47].

The pyrolysis oil in this research was obtained from catalytic pyrolysis of pinyon juniper (PJ) wood. PJ woodlands occupy about 30 million hectares in the western United States (including states of Arizona, California, Colorado, Idaho, Utah, Nevada, New Mexico, Oregon, and Wyoming). Domination of PJ woodlands decreases the herbaceous vegetation and increases bare lands, thus causing soil erosion and nutrition loss [24]. Studies have shown that expansion of PJ woodlands has reduced the amount of precipitation, increased soil erosion, and increase the potential of crown fires, hence, land management agencies are reducing the population of PJ woodlands [48–51]. In principle, PJ can become a potential biomass feedstock for production of bio-oil.

In view of its strong stability, sintering resistance, and poisoning resistance, it is expected that RM can serve as a promising catalyst support for HDO of bio-oil. Moreover, it is much cost-effective in comparison with other catalyst supports such as Al_2O_3, SiO_2, and TiO_2 which require complicated preparation procedures. Since silica and alumina are two major compounds of RM, commercial Ni/SiO_2-Al_2O_3 was tested in HDO process for comparison. Unlike traditional HDO catalysts (CoMo/Al_2O_3 and NiMo/Al_2O_3), this catalyst does not need any pre-treatments such as sulfidation and it can be used as received [12]. This catalyst is relatively cheaper than typical noble metal catalysts that are widely used for HDO reactions.

2. Material and methods

2.1. Material

PJ biomass chips were supplied by the U.S. Bureau of Land Management. RM was used as catalyst for fast pyrolysis of the PJ biomass. The wet red mud was dried at room temperature, reformulated and then ground and sieved to a particle size of 125 − 180 μm. The ground particles were calcined at 550 °C in a muffle furnace (Thermo Fisher Scientific, Waltham, MA) for 5 h before being used for the pyrolysis. The detailed characterization of the RM has been reported by Yathavan and Agblevor [24]. Analytical grade nickel nitrate hexahydrate ($Ni(NO_3)\cdot 6H_2O$) was purchased from Alfa Aesar (Haverhill, MA, USA). High purity (99%) hydrogen (Airgas, PA, USA) was used for HDO experiments. Commercial Nickel on silica/alumina (~65 wt% loading Ni) catalyst powder, obtained from Sigma-Aldrich (St. Louis, MO, USA), was used (as received) in HDO experiments for comparison.

2.2. Pyrolysis of biomass

PJ biomass chips ground to pass a 2-mm mesh were used as feedstock for production of catalytic pyrolysis oil. The pyrolysis was carried out in a pilot plant bubbling fluidized bed reactor described in detail by Mante and Agblevor [52]. At feeding rate of 0.9 kg/h (2 lb/h), catalytic pyrolysis oil was produced at 400 °C using RM catalyst. The pyrolytic products were condensed using a series of two ethylene glycol-cooled condensers and an electrostatic precipitator (ESP) operating at 30 kV. Details of the pyrolysis pilot plant can be found elsewhere [52].

2.3. Preparation of Ni/RM catalysts and characterization

Ni/RM catalysts were prepared at different concentrations of nickel using wet impregnation method [53,54]. At room temperature the calculated amount of $Ni(NO_3)\cdot 6H_2O$ was dissolved in 100 ml deionized water and then mixed with RM (particle size < 90 μm). The mixture was heated to 70 °C and continuously stirred for 5 h to prepare the catalyst precursor. The catalyst precursor was dried at 105 °C for 10 h and then calcined at 620 °C for 5 h. The catalyst precursor was reduced for 6 h at 450 °C using a reducing gas mixture of 10% H_2 and 90% N_2 at flow rate of 20 ml/min to obtain the tested catalyst, which was designated as x wt.% Ni/RM (x = 10, 20, 30, 40, 50, 65).

The BET (Brunauer-Emmet-Teller) surface area of Ni/RM catalysts were determined on a MS-16 BET analyzer (Quantachrome Instruments, Boynton Beach, FL, USA). About 0.1 g catalyst sample was used in each measurement. All samples were degassed at 300 °C for 4 h prior to duplicate simultaneous measurements. A standard porous Al_2O_3 sample was analyzed along with each run to ensure consistency between the different samples.

TG-TPR (Thermogravimetric-temperature programmed reduction) studies were carried out using a TGA Q500 (TA Instruments, Lindon, UT, USA). Twenty-five milligrams of catalyst (calcined form) was heated in a flow of 10% H_2/90% N_2 (20 ml/min) from room temperature to 700 °C at a heating rate of 10 °C/min. Hydrogen uptake was monitored by the change of sample weight according to the plot of derivative weight vs. temperature.

X-ray powder diffraction (XRD) analyses were carried out by Hazen Research Inc. (Golden, CO, USA). The samples were pulverized by hand in a mortar and pestle with isopropyl alcohol and analyzed using a Bruker D8 Advance with Davinci design and a Lynxeye detector. The pattern was measured in the interval from 5 to 85 in 2Θ using a 0.02 step size and 40 s of counting time.

Scanning electron microscopy (SEM) analysis was conducted on a FEI Quanta FEG-650 (Thermo Fisher Scientific, MA, USA). For preparation of the specimens a small amount of catalyst was placed on a two-sided sticky tape resting on an aluminum holder and observed at different magnifications. Images were recorded using low vacuum secondary electron (LFD) detector.

For inductively-coupled plasma (ICP) analysis, 0.5 g catalyst sample was digested in nitric acid at 95 °C for 1 h. Then 12 ml 30 wt.% hydrogen peroxide was added to the digestion tube and cooled to room temperature [55]. The extracts were measured using a Thermo iCAP 6300 ICP-OES Inductively-Coupled Plasma Spectrophotometer (Thermo Fisher Scientific, MA, USA) with Optical Emission.

2.4. Hydrodeoxygenation of bio oil

The bio-oil was subjected to HDO reactions in a Parr Series 4560

300 ml autoclave reactor (Parr Instruments, Moline, IL, USA). The reactor can withstand a maximum pressure of 14 MPa at 500 °C. A Parr 4848 controller was used to control the internal temperature and impeller speed. In a typical test, bio-oil (20 g) and catalyst (3 g) were loaded into the reactor. The reactor was first flushed with nitrogen three times and then flushed with hydrogen three times to purge the reactor. High purity hydrogen was supplied from a reservoir tank via a pressure regulator. The reactor was then pressurized with hydrogen to 6.2 MPa and a gas sample was taken from a gas release valve from the gas sampling port for gas analysis when the reactor was at room temperature. The reactor was then heated to reaction temperature (400 or 450 °C) at heating rate of 15 °C/min using a heating mantle. The reaction time was recorded when the required temperature was reached. The stirrer speed was kept constant (~1000 rpm) in all experiments.

After the desired reaction time (30 min), the reactor was cooled to room temperature using the internal cooling coil. A gas sample was collected in a tedlar bag for gas analysis when the reactor was cooled down to room temperature. Hydrogen consumption was measured using Eq. (1).

$$H_2\ consumption\left(\frac{\text{mole } H_2}{g\ biooil}\right) = (n_{iH2} - x_{f_{H2}}.\ n_{f_{tot}}) \times \frac{1}{20\,g\ biooil} \quad (1)$$

Where n_{iH2} is the initial number of mole of hydrogen, $x_{f_{H2}}$ is the final mole fraction of hydrogen, and $n_{f_{tot}}$ is the total number of mole of gas at the end of experiment.

After each experiment, the liquid products were collected in centrifuge tubes and centrifuged (using a 5702 R centrifuge, Eppendof, Germany) for 30 min at g-force of 2147 to separate the resulting aqueous and organic phases and residual solids and catalyst. Both liquid phases were separated and weighed for mass balance determination. The solids (catalyst and coke) were collected and dried at 95 °C for 6 h. The vessel and reactor parts were rinsed with methanol-toluene mixture (1:1 vol. ratio) to collect any remaining catalyst and oil. The solvent washings were filtered through Watman 42 ashless filter paper (GE Healthcare, UK) and dried at 95 °C. The weight of filter paper was recorded before and after filtration.

The total mass of gaseous product was calculated using Eq. (2):

$$W_g = \sum_i x_i.\ MW_i.\ n_{tot} \quad (2)$$

Where W_g is the total mass of gaseous product (g), x_i is the mole fraction of gas i, MW_i is the molecular weight of gas i (g/mole), and n_{tot} is the total number of moles of gas product. The yield of liquid, gas, and solid product were calculated using Eqs. (3)–(5) respectively.

$$Y_{liquid}(\%) = \frac{W_l}{W_f} \times 100 \quad (3)$$

$$Y_{gas}(\%) = \frac{W_g}{W_f} \times 100 \quad (4)$$

$$Y_{coke}(\%) = \frac{(W_s - W_C)}{W_f} \times 100 \quad (5)$$

Where W_f is the mass of feed bio-oil and consumed hydrogen combined (g), W_l is the mass of liquid product (g), W_g is the mass of gas product (g), W_s is the weight of total solid residues (g), and W_c is the weight of catalyst (g).

An elemental carbon balance before and after each experiment was performed.

In a blank experiment, without catalyst, 20 g of PJ bio-oil was charged into the reactor and the reactor was pressurized to 6.2 MPa with hydrogen. The bio-oil was allowed to react for 30 min at 400 °C. All experiments were conducted in triplicate.

2.5. Characterization of PJ wood, catalytic pyrolysis oil, and HDO products

2.5.1. Physical properties

The moisture content of the PJ wood was determined according to standard method ASTM E1756- 08 and the ash content was determined according to ASTM E1755-01 method. The water content of the crude bio-oil and hydrotreated oil were determined by Karl-Fisher titration method with Hydranal® -composite 5 solution. A Metrohm 701 KF Titrino and 703 titration stand setup (Brinkmann Instruments, Riverview, FL, USA) were used for the volumetric Karl Fischer titration. The pH was measured using Mettler Toledo pH Meter and probe (Mettler − Toledo GmbH, Switzerland). The density and kinematic viscosity of the bio-oil and HDO oil were measured at 40 °C using Anton Parr Stabinger viscometer svm 3000 (Ashland, VA, USA).

2.5.2. Chemical properties

The higher heating value (HHV) of PJ wood, bio-oil, and hydrotreated oil were determined using IKA Model C2000 basic bomb calorimeter (IKA Inc., Wilmington, NC, USA). The elemental composition of biomass, bio-oil, and hydrogenated oil were determined using Thermo Fischer Scientific Flash 2000 organic elemental analyzer (Thermo Fisher Scientific, Waltham, MA, USA). Fourier transform infrared spectrum (FT-IR) over the range of 600–4000 nm was recorded using Avatar 360 FT-IR instrument (Thermo Fisher Scientific, Waltham, MA, USA). The ^{13}C NMR spectra were recorded on a Bruker AvanceIII HD Ascend 500 MHz NMR spectrometer (Billerica, MA, USA). In a 5-mm sample probe about 0.5 g of oil was dissolved in 1.5 g deuterated solvent. Dimethyl sulfoxide-d_6 (DMSO-d_6) (Sigma-Aldrich, St. Louis, MO, USA) was used for catalytic pyrolysis oil and chloroform-d (Cambridge Isotope Laboratories, Inc., USA) was used for HDO oil. The observing frequency for the ^{13}C nucleus was 100.58 MHz, the pulse width was 10 μs, the acquisition time was 1.58 s, and the relaxation delay was 2 s. The spectra were obtained with 3000 scans and a sweep width of 20 kHz.

2.6. Gas analysis

Gas samples were collected in tedlar sampling bags from the sampling port installed on the reactor head and analyzed using a Varian 490-micro GC system (Agilent Technology, Santa Clara, CA, USA). The micro GC was equipped with two modules: a 10 m Molsieve 5 A (MS) column, and a 10 m porous polymer (PPU) column. Each module had a thermal conductivity detector. MS was used to analyze hydrogen, methane, and carbon monoxide (CO), while carbon dioxide (CO_2) and $C_1 - C_5$ hydrocarbons were analyzed on the PPU column. Gas concentrations were calculated relative to calibration curves of three standard gas mixtures supplied from Scotty Specialty Gases (Fremont, CA, USA). Gas samples were analyzed for H_2, CO, CO_2, CH_4, C_2H_4, C_2H_6, C_3H_8, C_4H_{10}, and C_5H_{12}.

3. Results and discussion

3.1. Characterization of PJ biomass and PJ pyrolysis oil

The biomass was characterized on the basis of moisture, ash content, elemental composition, and higher heating value (HHV) [56]. The physicochemical properties of the PJ wood are shown in Table 1. The ESP-condensed oil was used in HDO experiments because this was representative of all the oil fractions and had the least amount of water. The ESP oil was characterized for ash content, ultimate composition, HHV, pH, water content, density, and dynamic viscosity. The yield of organic liquid after catalytic fast pyrolysis of biomass was about 30% mass of fed PJ wood (dry basis). The physicochemical properties of the raw bio-oil are shown in Table 1. The ultimate composition was similar to those reported by Yathavan and Agblevor [24].

Table 1
Characterization of pinyon-juniper biomass and bio-oil[a].

Properties	PJ biomass	Catalytic PJ bio-oil
Elemental Composition (dry basis) (wt.%)		
Ash content	0.53 ± 0.06	0.00
Nitrogen	0.17 ± 0.01	0.47 ± 0.04
Carbon	54.43 ± 0.11	67.42 ± 0.21
Hydrogen	6.27 ± 0.09	7.23 ± 0.07
Sulfur	< DL[b]	< DL[b]
Oxygen[c]	38.60 ± 0.12	24.88 ± 0.12
HHV (MJ/kg)	19.37 ± 0.11	28.41 ± 0.23
pH	NA	3.27 ± 0.05
Water content (wt.%)	6.65 ± 0.09	3.36 ± 0.08
Density (g/cm^3)	0.55 ± 0.03	1.16 ± 0.02
Dynamic viscosity (cP)	NA	95.5 ± 1.5

[a] Error are the standard deviation of two measurements.
[b] Below detection limit.
[c] By difference.

3.2. Characterization of Ni/RM catalysts

The BET specific surface area of RM was relatively low after calcination (37.51 m^2/g), but after reduction of the calcined RM it increased to 54.34 m^2/g. The increase in surface area was attributed to elimination of oxygen during the reduction.

The variation of BET specific surface area of Ni/RM catalysts vs. nickel loading is shown in Fig. 1. The specific surface area of the catalysts increased due to the reduction of NiO to Ni and formation of pores [57–60]. By increasing the nickel content from 10% to 65%, the BET surface area of the activated catalyst increased from 45.47 to 88.36 m^2/g. The increase in surface area with increase in nickel loading was in good agreement with other researchers [61]. Linear regressions of BET surface area vs. nickel loading showed R^2 of 0.99 and 0.96 respectively for the calcined form and reduced forms of the catalyst. The increase in surface area with increase in Ni content suggests that nickel was efficiently dispersed on RM support with minimum pore plugging during impregnation [62].

TG-TPR was performed to investigate the reducibility of nickel oxide, RM support, and the interaction between nickel and the RM support (Figs. S1–S8 in Supplementary data show the TPR profile of individual samples). For comparison, TPR profiles of NiO, 40% Ni/RM catalyst, and RM support are shown in Fig. 2. TPR profile of RM indicated three major reduction peaks at 279, 542, and 694 °C (Figs. 2 and S1 in Supplementary data). The peak at 279 °C could be due to the reduction of Fe_2O_3 to Fe_3O_4 and the unresolved peaks centered at 542 °C and 694 °C could correspond to reduction of Fe_3O_4 to FeO and then to elemental Fe [23].

The TPR profiles of Ni/RM catalysts appeared to show strong interaction between the RM and NiO since the RM TPR peaks were reduced to two major reduction peaks assigned as lower temperature

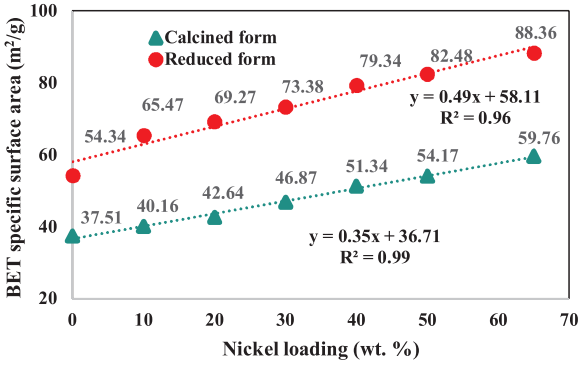

Fig. 1. BET surface area of Ni/RM catalysts vs. nickel content in calcined and reduced forms.

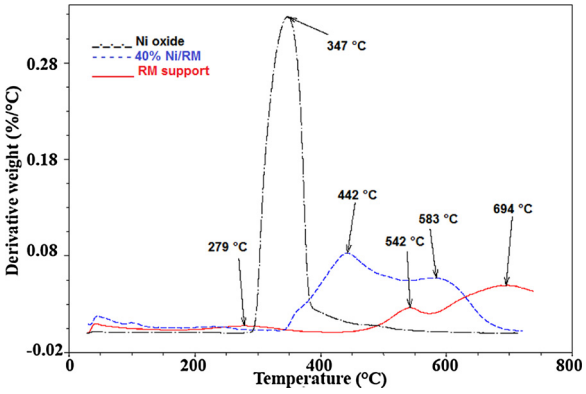

Fig. 2. TG-TPR profile of RM support, 40% Ni/RM, and Ni oxide.

Table 2
Reduction temperatures of Ni/RM catalysts according to TPR profiles.

Catalyst	Lower temperature peak (°C)	Higher temperature peak (°C)
10% Ni/RM	569	678
20% Ni/RM	540	668
30% Ni/RM	509	597
40% Ni/RM	442	583
50%Ni/RM	426	560
65% Ni/RM	412	486

peak and higher temperature peak as summarized in Table 2. There were no independent peaks of RM and NiO. The lower temperature peak appeared to have higher concentration of NiO than the higher temperature peak since its intensity increased with increased Ni content and its reduction temperature shifted towards that of nickel oxide (347 °C according to Figs. 2 and S8 in Supplementary data). This observation is in agreement with Jeangros et al. who observed interaction between SiO_2 and NiO during the reduction of NiO to Ni [58]. The intensity of the higher temperature peak decreased as Ni loading increased, but its reduction temperature also decreased with increased Ni content. The improvement in oxide catalyst reducibility (lower reduction temperature) with increase in metal content was attributed to interaction between the red mud support and NiO and has been reported for other oxide catalysts [60–68)]. In the case of 40 and 50% Ni, small shoulders were detected between 350 and 400 °C, 400 and 450 °C and an unresolved peak at about 580 °C appeared in TPR profile of 65%Ni/RM. This seems to indicate that there are different NiO species that interacted differently with RM [69].

Since the 40%Ni/RM catalyst performed best in terms of HDO reaction (described in details in Section 3.3), this catalyst was further characterized by ICP, XRD, and SEM. In order to investigate the effect of RM support and to verify the estimated amount of Ni added to the RM, ICP analyses were performed on RM and 40%Ni/RM catalyst. As shown in Table 3, the major metals present in RM were Al (9.08%), Ca (1.2%), Fe (21.56%), Na (7.17%), and Si (4.35%) and trace amounts of other metals such as As, Cd, Cu, Mo, Zn and others. RM (in reduced form) was investigated in HDO experiment to determine the effect of support on the chemical reactions. The results of RM effect are presented in Section 3.3. After impregnation of RM with nickel, the relative amounts of all metals decreased due to presence of 40% nickel. The ICP analysis of 40%Ni/RM showed a Ni content (40.8%), which was very close to the estimated amount added to the substrate.

Fig. 3 depicts the XRD patterns of fresh Ni/RM catalyst at different stages of processing and use. Distinct sharp peaks observed at 2Θ of 52.2°, 61° were attributed to metallic Ni produced from the reduction of NiO. The detection of NiO peaks in reduced 40%Ni/RM (2Θ of 43.7°, 50.9°, and 74.7°) showed that nickel oxide was not completely reduced to elemental Ni after the hydrogen treatment, perhaps because of mass

Table 3
ICP analysis of RM support and 40%Ni/RM catalyst.

Metal (wt.%)	RM	40%Ni/RM
Al	9.08	4.44
Ca	1.20	0.65
Fe	21.56	9.47
K	0.03	0.02
Mg	0.07	0.04
Na	7.17	3.51
Ni	< 0.01	40.8
P	0.03	0.01
S	0.10	0.06
Si	4.35	2.53
Metal (mg/kg)	**RM**	**40%Ni/RM**
As	0.87	< DL
B	9.41	0.85
Ba	10.4	4.55
Cd	5.79	3.37
Co	278	12.3
Cr	245	132
Cu	3.13	< DL
Mn	< DL	< DL
Mo	1.62	0.48
Pb	156	7.09
Se	< DL	< DL
Sr	23.1	2.28
Zn	2105	26.1

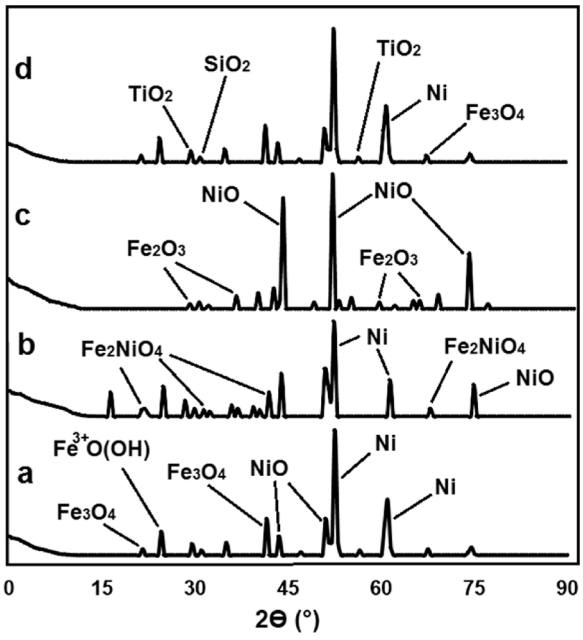

Fig. 3. XRD patterns of a) fresh 40%Ni/RM HDO catalyst, b) used 40%Ni/RM catalyst (after HDO process), c) regenerated 40%Ni/RM catalyst after burning off the coke, and d) regenerated and reduced 40%Ni/RM HDO catalyst.

transfer limitations (Fig. 3a) and temperature effect. It has been reported that complete reduction of NiO does not occur until the reduction temperature was above 600 °C [58], which appears to corroborate the current data, since the reduction temperature was 450 °C. The magnetite (Fe_3O_4) peaks detected in the spectrum were due to the reduction of hematite (Fe_2O_3) that was present in the RM [24].

The XRD pattern of used 40%Ni/RM (Fig. 3b) catalyst showed stronger NiO peaks compared to the fresh catalyst, suggesting that some Ni was oxidized during HDO. This could be one reason for the partial deactivation of the catalyst. Additionally, trevorite (Fe_2NiO_4) peaks were also observed after HDO, which could also contribute to the deactivation of active Ni sites. Furthermore, the intensities of Ni peaks (2Θ of 52.1° and 61°) in the used catalyst were lower than those of the fresh catalyst, suggesting that there was overall deactivation of the catalyst.

In order to recycle the catalyst, the used catalyst was regenerated in a muffle furnace at 400 °C for 4 h to burn off the deposited carbonaceous compounds (coke), which was followed by reduction as described in material and methods section. The XRD pattern of the regenerated catalyst (Fig. 3c) showed strong NiO diffraction peaks at 2Θ of 43.9°, 50.8°, and 75°, which were due to the oxidation of nickel into NiO under heat treatment in air. Furthermore, it was interesting to note the weak Ni diffraction peaks in the XRD pattern of the regenerated catalyst (Fig. 3c). It suggested mass transfer limitation of oxygen, which could not penetrate the bulk RM to oxidize the Ni buried in it. The detection of hematite (Fe_2O_3) diffraction peaks in the regenerated catalyst was ascribed to oxidation of magnetite.

When the regenerated catalyst was activated by reduction in H_2, its XRD pattern (Fig. 3d) showed similar diffraction peaks as the fresh catalyst (Fig. 3a) suggesting complete recyclability of the catalyst. More detailed information on catalytic activity of the used catalyst and the recycled catalyst are discussed in Section 3.4.

The surface morphology of the catalyst was studied using scanning electron microscopy (SEM). The SEM images of the RM support, 40% Ni/RM catalyst precursor (calcined form), fresh 40%Ni/RM catalyst (reduced form), and used 40% Ni/RM catalyst are presented in Fig. 4. In the case of RM support (Fig. 4a), in addition to amorphous looking particles, crossed-cocentric discs and spherical-shaped particles were observed. Nickel oxide particles were dispersed in the RM support (Fig. 4b) in small clumps. Ni particles with relatively uniform morphology and approximate mean diameter of 90 nm were dispersed on the surface of the RM in the case of activated Ni/RM (Fig. 4c). The SEM picture for the used catalyst (Fig. 4d) showed that the catalyst was coated with coke after HDO process, which could affect the hydrogen transfer to active sites and also reduce catalyst activity.

3.3. Results of HDO experiments

3.3.1. Mass balance of HDO products

No catalytic activity was observed in the case of blank experiments and the bio-oil polymerized (solidified) due to the presence of highly reactive compounds in bio-oil such as sugar derivatives and phenolic compounds [70]. The reactor was not catalytically active and did not influence the experiment.

As expected, Ni loading had significant effect on HDO product yields distribution (Fig. 5). HDO experiment using RM (0% Ni loading) produced 48.2% solids (coke) and 43.4% gas and only 5.2% organic liquid. About 60.8% of the original carbon was recovered in the solid residues, 31.2% was converted to gaseous products and only 5.3% was retained in the organic liquid product (Table 4). These results suggested that at 0%Ni loading, cracking and coke formation reactions were dominant compared to HDO reactions, hence, the RM support had very limited activity for HDO reactions but favored unwanted side reactions (coke and gas formation) in the absence of Ni.

When the Ni loading was increased from 10% to 40%, the organic liquid yield increased from 26.1% to 68.6%, the gas yield decreased from 35.2% to 16.4%, and the coke yield decreased from 34.5% to 4.2% (Fig. 5). These results showed that increasing the Ni content improved HDO reactions and reduced coke formation and cracking reactions. Furthermore, the water yield increased from 2.2% to 9.1% indicating higher levels of HDO reactions that produced water. At Ni loading of 50% and 65% the organic liquid yields were 64.3% and 56.3% respectively and no significant changes were observed in coke yield. However, the gas yield increased to 19.1% and 25.5% respectively for Ni contents of 50% and 65%. Comparing the product yields distribution of the HDO experiments using 40, 50, and 65% Ni loading, it was concluded that HDO reactions for organic liquid were optimal at this

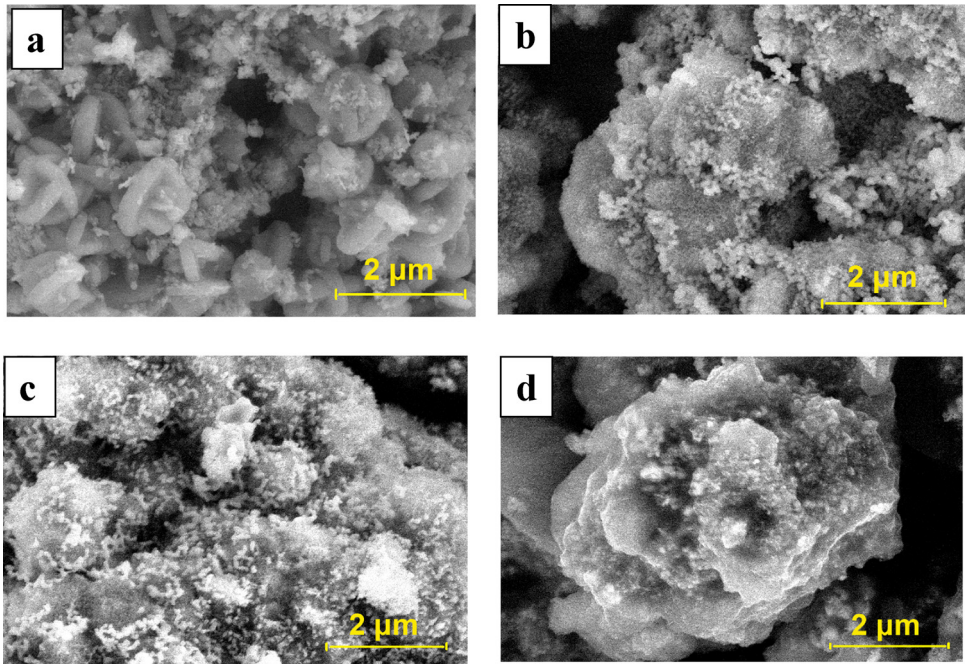

Fig. 4. SEM images of Ni/RM catalyst at different stages: a) RM support, b) 40%Ni/RM (calcined form), c) 40%Ni/RM (reduced form) (fresh catalyst for HDO), d) used 40%Ni/RM catalyst after HDO process (coked catalyst).

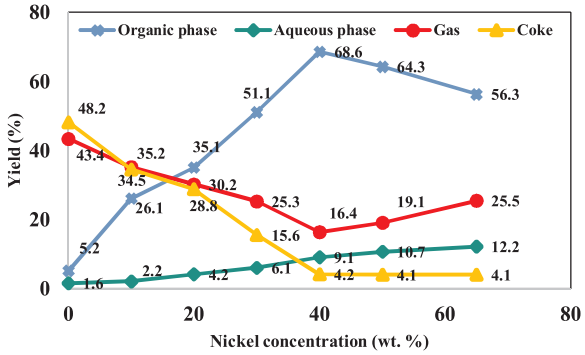

Fig. 5. Effect of nickel concentration on HDO products (organic phase (HDO oil), aqueous phase (mostly water), gas, and coke) yield distribution (dry basis) using Ni/RM catalyst.

reaction time (30 min) using 40%Ni/RM. The higher Ni loadings of 50% Ni and 65%Ni did not improve organic liquid production, but rather caused increased hydrocracking, which generated higher amounts of gas products. The physicochemical properties of the HDO oil such as elemental composition and HHV did not change significantly when Ni content increased from 40% to 50% and 65% (Table 5). In contrast, H_2 consumption increased due to higher levels of hydrocracking of HDO oil compounds and methanation of CO_2 and CO.

The aqueous liquid (water) yield was 10.7% and 12.2% at Ni loadings of 50% and 65% respectively (Fig. 5), indicating slight increases compared to that of 40%Ni/RM (9.1%). This result is further explained in Section 3.3.2. The highest fraction of original carbon (84%) retained in the organic liquid product was achieved when 40% Ni/RM was used for HDO experiment (Table 4). At this Ni loading, 9.5% of the initial carbon was converted to gas, and only 5.3% remained in the coke.

3.3.2. Characterization of HDO products

3.3.2.1. Physicochemical properties of HDO products. Changes in properties of HDO liquid and gas products composition at different Ni loadings are reported in Table 5. At 0%Ni (using only RM support), the carbon, hydrogen, and oxygen contents of the organic phase were 68.16, 7.58, and 23.54 wt.% respectively. The elemental composition changed slightly compared to 67.42, 7.23 and 24.88 wt.% of C, H, and O respectively of the original bio oil (Table 1), which, suggested there were minimal HDO reactions on the RM support. The RM support favored cracking and coke formation reactions and was considered as an inert support for the HDO reactions.

Increasing the Ni content from 10% to 40% significantly increased the hydrogen content of the organic HDO product from 9.56 wt.% to 15.83 wt.% while oxygen content was reduced from 19.72 wt.% to 1.35 wt.%. Hydrogen consumption increased from 0.021 mol/(g bio-oil) to 0.053 mol/(g bio-oil) when Ni loading increased from 10% to

Table 4
Total mass balance and carbon mass balance of HDO products at different nickel contents.

Ni loading (wt.%)	Total mass balance (wt.%)					Carbon balance (wt.%)				
	Organic	Aqueous	Gas	Coke	SUM	Organic	Aqueous	Gas	Coke	SUM
0	5.2	1.6	43.4	48.2	98.4	5.3	1.4	31.2	60.8	98.6
10	26.1	2.2	35.2	34.5	98.0	27.2	1.1	26.8	43.5	98.6
20	35.1	4.2	30.2	28.8	98.3	38.8	0.6	22.4	36.3	98.1
30	51.1	6.1	25.3	15.6	98.1	58.7	0.3	19.3	19.7	98.0
40	68.6	9.1	16.4	4.2	98.3	84.0	0.0	9.5	5.3	98.8
50	64.3	10.7	19.1	4.1	98.2	78.9	0.0	14.2	5.2	98.3
65	56.3	12.2	25.5	4.1	98.1	69.4	0.0	23.7	5.2	98.3

Table 5
H_2 consumption, physicochemical properties of the liquid products, and gas product composition at different nickel concentrations using Ni/RM catalyst.

Properties	Temperature and reaction time were 400 °C, and 30 min respectively						
	RM	10% Ni/RM	20% Ni/RM	30% Ni/RM	40% Ni/RM	50% Ni/RM	65% Ni/RM
H_2 consumption (mol/g bio-oil)	0.002	0.021	0.035	0.046	0.053	0.061	0.072
Aqueous phase							
Water content (wt.%)	71.35	80.36	85.67	97.45	99.45	99.50	99.95
pH	4.11	4.35	5.47	6.36	6.91	6.93	6.93
HDO oil (organic phase)							
Elemental composition (dry basis) (wt.%)							
N	0.45	0.38	0.33	0.32	0.31	0.30	0.30
C	68.16	70.34	74.56	77.49	82.52	82.71	83.11
H	7.85	9.56	11.32	13.45	15.82	16.13	16.59
O	23.54	19.72	19.37	8.74	1.35	0.86	0
HHV (MJ/kg)	29.15	35.56	38.38	41.73	45.77	45.79	45.81
pH	3.65	4.23	5.04	5.78	NA	NA	NA
Water content (wt.%)	3.24	2.11	1.07	0.67	< DL[a]	< DL[a]	< DL[a]
Density (g/ml)	1.11	0.93	0.88	0.82	0.79	0.78	0.78
Dynamic viscosity (cP)	88.54	12.45	8.56	3.67	1.37	1.31	1.31
Gas composition (mole %)							
CO	12.11	6.02	5.28	4.37	3.32	2.84	2.23
CO_2	16.43	13.47	9.17	7.56	5.52	4.75	4.19
CH_4	43.77	54.15	59.75	61.36	67.34	68.26	69.76
C_2H_4	5.34	7.26	7.89	8.11	8.26	8.41	8.66
C_3H_8	10.21	9.34	8.55	7.78	7.56	7.61	7.67
C_4H_{10}	7.42	6.32	5.83	5.62	5.45	5.40	5.28
C_5H_{12}	4.35	3.41	3.34	3.16	2.47	2.32	2.19

[a] The detection limit was 0.05%.

40% (Table 1). As a critical scale-up parameter, the hydrogen consumption at Ni loading of 40% was slightly higher than the value reported by Agblevor et al. using sulfided cobalt/molybdenum oxide supported on zirconia [71]. The density of the oil was reduced by about 15% from 0.93 g/cm^3 to 0.79 g/cm^3 when the Ni loading increased from 10% to 40%. The dynamic viscosity decreased from 12.45 cP to 1.37 cP over this Ni loading range. The reduction in density and viscosity could be attributed to hydrocracking of high molecular weight compounds in the bio-oil during HDO [72,73]. The reduction in acidity can be due to conversion of carboxylic acids in the bio-oil to other compounds during hydrodeoxygenation [74]. At Ni loadings of 50% and 65% the changes in elemental composition of HDO oils were not significantly different from that of 40% Ni loading (Table 5), however, the hydrogen consumptions were 0.061 mol/(g bio-oil) and 0.072 mol/(g bio-oil) respectively. These results suggest that increased catalyst activity at 50% and 65% Ni loadings increased the rate of hydrocracking and methanation rather than HDO reactions as previously mentioned (Fig. 5). Furthermore, no significant changes were observed in the viscosity of HDO oil at Ni loadings of 50% and 65% compared to that of 40%Ni/RM.

In all HDO experiments, the major gas product was methane (Table 5). The concentration of methane increased from 54.15 mol% to 67.34 mol% when the Ni loading increased from 10% to 40%. Increasing the Ni loading decreased the concentration of CO and CO_2, because of methanation of these two gases due to increased catalyst activity [74–76]. The concentration of C_3-C_5 gases gradually decreased with increase in Ni content, which could be due to hydrocracking of these gases at higher Ni loadings. Increasing the Ni content from 40% to 50% and 65% increased the concentration of methane from 67.34 mol% to 68.26 mol% and 69.76 mol% respectively while CO and CO_2 decreased to 2.84% and 4.75% respectively at 50% Ni loading and 2.23 mol% and 4.19 mol% respectively at 65% Ni loading.

3.3.2.2. FT-IR analysis of HDO organic liquids. The FT-IR spectra of the raw bio-oil and HDO oils at different Ni loadings are shown in Figs. S9–S16 (Supplementary data). For comparison, the FT-IR spectra of the raw bio-oil and the HDO oil obtained from 40%Ni/RM are shown in Fig. 6. The absorbance peaks between 3050 and 3650 cm^{-1} were assigned to −OH stretching vibration, which indicated that phenolic compounds, carboxylic acids, water, and alcohols were produced during catalytic pyrolysis of PJ biomass. With the increase in Ni loading, the intensity of these peaks gradually decreased or even disappeared in the HDO oil, which could be due to phenolic or alcoholic hydroxyl cleavage, elimination, intramolecular dehydration, or hydrodeoxygenation of −OH groups. Furthermore, during HDO, water could possibly migrate to the aqueous phase. The peaks between 2840 and 3010 cm^{-1} and the two other bands at 1376 and 1453 cm^{-1} were assigned to C−H stretching and deformation in methyl groups and methylene groups, respectively. The peaks intensified after HDO compared to the original bio-oil. The peaks at 1590–1610 cm^{-1} were attributed to benzene in-ring C−C stretching. These peaks decreased gradually with increasing Ni loading suggesting that the aromatics possibly underwent cracking, ring saturation, or polymerization to form coke. The peak at 1670 cm^{-1}, which was assigned to C=O stretching, gradually decreased with increase in Ni loading.

The appearance of typical carbonyl group C=O stretching

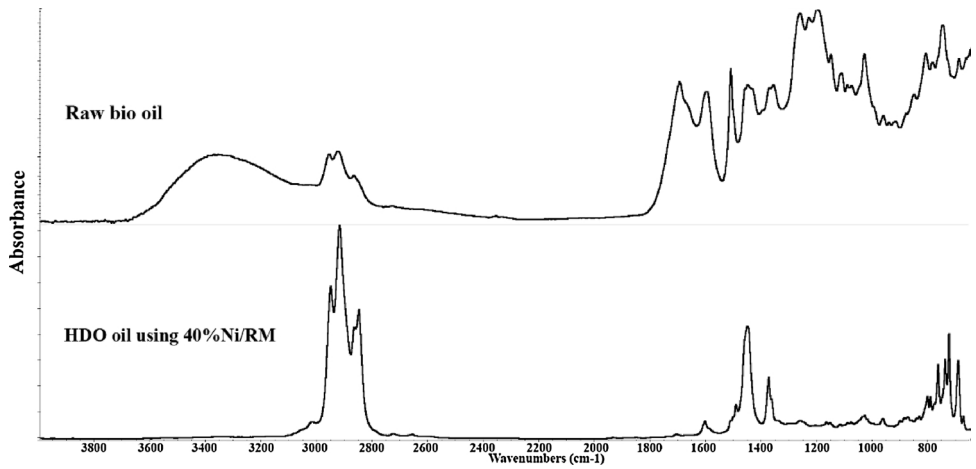

Fig. 6. FT-IR spectra of raw bio oil and HDO oil using 40%Ni/RM catalyst.

vibrations at 1710 cm^{-1} showed that aldehydes or ketones were significant at 10% Ni loading, while at higher loadings, these peaks disappeared. Similarly, at higher Ni loadings the C—O stretching absorption band at 1033 and 1100 cm^{-1} disappeared, which could be due to the deoxygenation of alcohols, phenols, or esters. The peaks between 740 and 830 cm^{-1} assigned to C—H out-of plane bending vibration from aromatics and their derivatives decreased gradually because of hydrogenation of the benzene ring. These results indicated that the oxygenated groups (—OH, C═O, and C—O) were significantly removed from the HDO oil. At 40% Ni loading, mostly hydrocarbon peaks were present as indicated by the peaks between 2840 and 3010 cm^{-1} and the two other bands at 1376 and 1453 cm^{-1} due to C—H stretching; the 1600 cm^{-1} due to aromatics; the 730–770 cm^{-1} due to mono-substituted C–H bend; and o, m, p- distributed C–H bend peaks between 735–840 cm^{-1} (Fig. 6). Compared to the FT-IR spectrum of the raw bio-oil, the HDO oil of 40% Ni/RM indicated significant removal of oxygenated groups (Fig. 6) which corroborates the CHNOS analysis data in Table 5. At Ni loadings of 50% and 65% (Figs. S15 and S16 in Supplementary data), the aromatic peaks decreased significantly suggesting that there was increased hydrogenation of aromatics and/or hydrocracking of these compounds at higher catalyst activities compared to that of 40% Ni/RM. According to Fig. 6, it was clear that after HDO process, —OH peaks (at 3050 and 3650 cm^{-1}), C═O peaks (at 1670 cm^{-1} and1710 cm^{-1}), and C–O peaks (at 1033 and 1100 cm^{-1}) disappeared, whereas hydrocarbon peaks (C—C and C–H) increased significantly suggesting efficient removal of oxygen from the raw bio-oil.

3.3.2.3. ^{13}C NMR analysis of HDO organic liquids. The functional groups present in the crude bio-oil and HDO oils were characterized by semiquantitative integration of ^{13}C NMR spectra. The ^{13}C NMR spectra of the raw bio-oil, and HDO oils at different Ni loadings are shown in Fig. 7. The chemical shifts of various functional groups were assigned according to those reported in literature [54,73]. The semi-quantitative analysis of the ^{13}C NMR functional groups are presented in Table 6. The crude bio-oil had high amounts of carbohydrate degradation products, alcohols, ethers, methoxylated phenols, carboxylic groups, aldehydes, and ketones.

The characteristic peaks at 0–28 ppm assigned to saturated aliphatic carbon atoms increased during HDO due to hydrogenation of unsaturated aliphatics, HDO of alcohols, ethers, carboxylic acids, aldehydes, and ketones. Increasing the Ni loading from 10% to 40% increased the saturated aliphatic carbon atoms from 24.7% to 42.6% (Fig. 7 and Table 6) due to improved hydrogenation/hydrodeoxygenation of unsaturated compounds and oxygenated compounds.

The chemical shifts of 28–55 ppm assigned to the unsaturated carbon atoms that are separated from oxygen atoms by at least two bonds [77,78], were present in the bio-oil and its content in the HDO oil increased as the Ni content of the catalyst increased. The chemical shifts of 55–95 ppm were assigned to aliphatic carbon atoms attached to oxygen atoms in alcohols, esters, and anhydrous carbohydrates. Increasing Ni loading, decreased the amount of alcohols, esters, and anhydrous carbohydrates due to increased catalyst activity. At Ni loadings of 40%, 50% and 65% no peaks were observed at chemical shifts between 55–95 ppm (Fig. 7 and Table 6) suggesting that there was complete deoxygenation of all the oxygenated compounds including the methoxy carbon that resonates at 55–57 ppm.

The characteristic peaks at chemical shift of 95–165 ppm were assigned to aromatic carbon atoms in phenolic compounds and furans. These carbon atoms decreased with increasing Ni loading due to hydrogenation/deoxygenation of these compounds. When Ni loading was increased from 40% to 65%, unsaturated aliphatics increased from 17.6% to 27.6% and aromatic compounds decreased from 39.8% to 16.2%. These results could be due to partial hydrogenation of aromatic compounds. The saturated aliphatics content increased from 42.6% to 56.2% due to increased hydrogenation of unsaturated aliphatics (Fig. 7 and Table 6). However, hydrogenation of unsaturated aliphatics was not complete even at 65% Ni loading. Longer reaction times could result in complete hydrogenation of unsaturated aliphatic carbons, but longer reaction times are known to cause hydrocracking of organic compounds to gases, which will reduce the organic liquid yield [12,73].

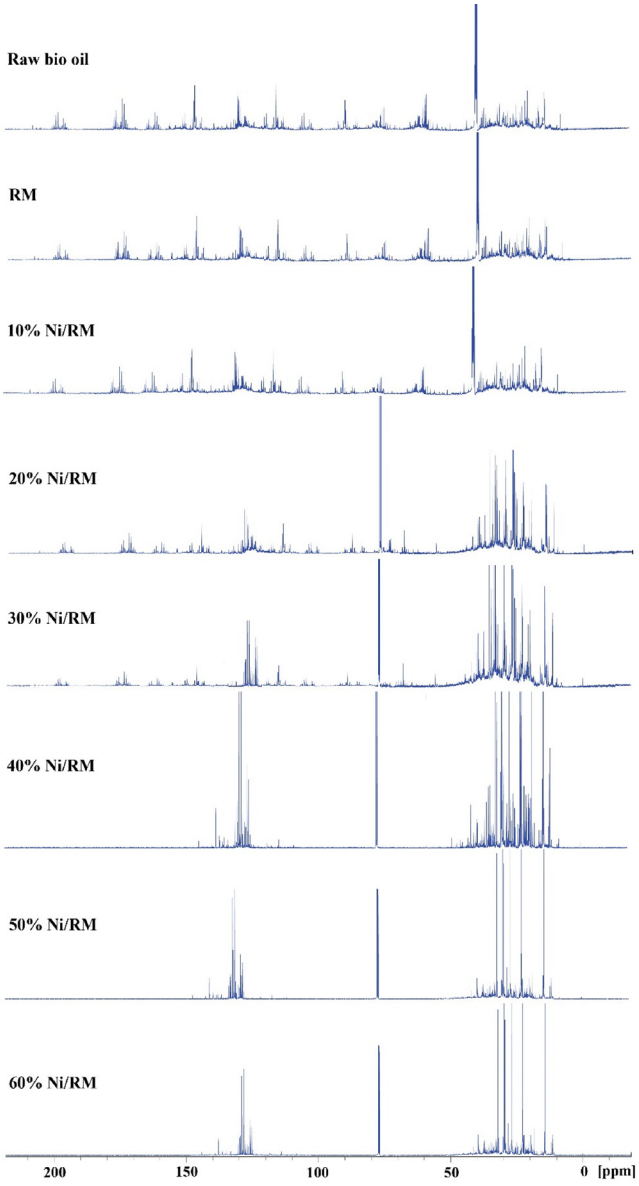

Fig. 7. ^{13}C NMR spectra of raw bio oil and HDO oils at different Ni concentrations.

The chemical shifts at 165–180 ppm assigned to carboxylic acids and esters, decreased gradually and finally disappeared at high Ni loadings. Increasing the Ni loading from 10% to 30%, decreased these carboxylic carbon signals intensity from 5.3% to 1.4%. At higher Ni loadings, no characteristic peaks were observed between 165–180 ppm (Fig. 7 and Table 6), because of complete deoxygenation of these compounds.

Characteristic chemical shifts of 180–215 ppm assigned to carbon atoms of carbonyl groups (aldehydes and ketones) decreased from 4.8% in bio-oil to zero in HDO oil at 40% Ni loading indicating that aldehydes and ketones were completely deoxygenated.

3.4. Catalyst deactivation and regenerability

The 40%Ni/RM was used to investigate catalyst deactivation and

Table 6
Functional group distribution of crude bio-oil and HDO oils at different nickel concentrations from ^{13}C NMR spectral integration.

Chemical shift region (ppm)	Dominant type of carbon	Percentage of carbon based on ^{13}C NMR analysis							
		Feed bio-oil	RM	10% Ni/RM	20% Ni/RM	30% Ni/RM	40% Ni/RM	50% Ni/RM	65% Ni/RM
0–28	Saturated aliphatic groups	15.8	17.1	24.7	31.8	36.7	42.6	46.3	56.2
28–55	Unsaturated aliphatic groups	9.7	10.8	13.6	14.9	16.8	17.6	23.4	27.6
55–95	Alcohols, ethers, phenolic methoxys, anhydrosugars	15.4	14.8	11.3	8.4	4.2	0	0	0
95–165	Aromatics, Furans	45.7	44.6	41.5	40.9	40.1	39.8	30.3	16.2
165–180	Organic (carboxylic) acids, esters	8.6	8.2	5.3	2.1	1.4	0	0	0
180–215	Ketones, aldehydes	4.8	4.5	3.6	1.9	0.8	0	0	0

recyclability by conducting several HDO runs without any regeneration or reduction of the catalyst between runs. As shown in Fig. S17 in Supplementary data, the organic liquid yield decreased from 68.6% to 6.8% after three consecutive batches while the gas yield increased from 16.4% to 41.5% and the coke yield increased from 4.2% to 47.4%. The properties of HDO oil obtained from this set of experiments are summarized in Table S1 (Supplementary data). The physicochemical properties of the HDO oil after the third run was about the same as that of 0%Ni/RM HDO experiment (Table 5) which showed that the catalyst was completely deactivated after three suns. After the first HDO run, 4.2% coke formed on the catalyst (Fig. 5), but catalyst activity was drastically reduced during the second run and liquid yield was 51% and coke formation increased to 15%. Thus, coke formation may not be the main reason for catalyst deactivation [13]. As discussed in Section 3.2., irreversible adsorption of oxygen at active Ni sites as well as formation of trevorite (Fe_2NiO_4) could be other reasons for catalyst deactivation.

The spent catalyst was placed in muffle furnace to burn off the deposited coke at 400 °C for 4 h followed by reduction as described in Section 2.3. The regenerated/activated catalyst was then used in HDO experiments and the cycle was repeated five times. The product yields distribution using regenerated catalyst were almost identical as that of fresh 40%Ni/RM (Fig. 8). The physicochemical properties of the HDO oil obtained by using the regenerated catalysts were also consistent and about the same as that of fresh catalyst (Table 7). The yields of HDO oil obtained after five regenerations of Ni/RM catalyst were 68.1, 69.0, 67.5, 68.1, and 68.8% respectively (Fig. 8). These values were within 1% error from their average suggesting efficient regeneration of the catalyst (also see Table 7). Moreover, the coke yield was 4.1 ± 0.2% after catalyst regeneration experiments showing a good consistency between measurements, which showed reproducible catalyst regeneration/activation. These result indicated that the catalyst regained its activity after the regeneration/activation process. The regeneration of the commercial Ni/SiO_2-Al_2O_3 was not possible following the same procedure and the catalyst did not indicate HDO activity after reduction. Additionally, when exposed to air, the reduced commercial catalyst caught fire due to spontaneous oxidation, while the reduced Ni/RM was stable on exposure to air.

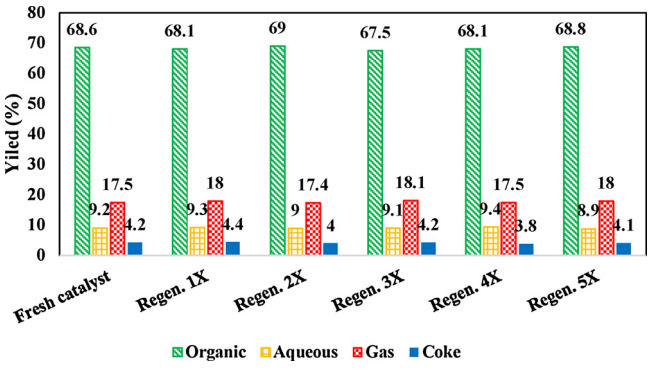

Fig. 8. Products yield distribution using regenerated 40% Ni/RM catalyst.

3.5. Comparison of catalytic activity of Ni/RM with commercial Ni/SiO_2-Al_2O_3

For comparison, commercial (~65%)Ni/SiO_2-Al_2O_3 (as received) was used in HDO experiments at reaction temperatures of 400 °C and 450 °C. Product yields distribution of HDO experiments using 40%Ni/RM (400 °C and 450 °C), 65%Ni/RM (400 °C and 450 °C), and commercial Ni/SiO_2-Al_2O_3 (400 °C and 450 °C) are shown in Fig. 9. The HDO oil properties obtained by using 40%Ni/RM at reaction temperature of 400 °C were similar to that of commercial Ni/SiO_2-Al_2O_3 at reaction temperature of 450 °C (Table 8). However, the organic liquid yield was much higher in the case of 40%Ni/RM (68.6%) than commercial Ni/SiO_2-Al_2O_3 (41.8%) (Fig. 9). The aqueous liquid yield in the case of 40%Ni/RM and commercial Ni/SiO_2-Al_2O_3 were 9.1% and 21.1% respectively (Fig. 9), which could be due to more methanation of CO and CO_2 over commercial Ni/SiO_2-Al_2O_3 (Table 8). The commercial Ni/SiO_2-Al_2O_3 produced more gas (27.6%) compared to 40%Ni/RM (16.4%) because of the higher activity of commercial Ni/SiO_2-Al_2O_3 for hydrocracking.

The 65%Ni/RM HDO oil yield was 41.3% at reaction temperature of 450 °C which was similar to the organic liquid yield obtained at the same temperature using the commercial catalyst (41.8% shown in Fig. 9). However, the yield of aqueous phase was higher, but the gas yield was lower because of increased methanation of CO_2 on the commercial catalyst (data not provided). The coke yield was also higher in the case of the commercial catalyst (7.3%) compared to 65%Ni/RM (5.5%) (Fig. 9). More details of HDO of PJ bio-oil using commercial Ni/SiO_2-Al_2O_3 has been reported elsewhere [12]. Overall, 40%Ni/RM catalyst produced higher organic liquid yield than the commercial catalyst, and HDO was performed at lower temperature (400 °C) than the commercial catalyst (450 °C) to obtain similar oil properties. The lower reaction temperature was beneficial in preventing hydrocracking and coke formation (Fig. 9). Hence, the prepared 40%Ni/RM could be an alternative to commercial Ni/SiO_2-Al_2O_3 catalyst and could be potentially less expensive than the commercial catalyst as reported previously [47].

4. Conclusion

Red mud, which is a waste material from the alumina industry, was used as support material for preparation of nickel hydrogenation/hydrodeoxygenation catalysts at different nickel loadings. Increasing the nickel content improved the catalytic activity of Ni/RM for HDO reactions. The highest organic liquid yield (68.6%) was achieved when 40%Ni/RM was used. The catalyst partially deactivated due to deposition of carbonaceous compounds (coke), oxidation of active nickel sites, and formation of trevorite (Fe_2NiO_4) during HDO. The Ni/RM catalysts demonstrated catalytic activity comparable to commercial Ni/SiO_2-Al_2O_3 at a lower nickel loading and lower reaction temperature. Overall, Ni/RM catalyst improved HDO reactions versus hydrocracking

Table 7
Properties of HDO oil using regenerated 40% Ni/RM catalyst.

Properties	Catalyst regeneration #					
	Fresh	Regen. 1X	Regen. 2X	Regen. 3X	Regen. 4X	Regen. 5X
H_2 consumption (mol/g bio-oil)	0.053	0.050	0.055	0.051	0.056	0.051
Elemental composition (dry basis) (wt.%)						
N	0.31	0.32	0.30	0.29	0.33	0.32
C	82.52	82.36	82.54	82.67	82.41	82.55
H	15.82	15.56	15.78	15.46	15.72	15.35
O	1.35	1.76	1.38	1.58	1.54	1.78
HHV (MJ/kg)	45.77	45.01	45.01	45.12	45.05	45.02
Dynamic viscosity (cP)	1.37	1.37	1.41	1.35	1.36	1.39

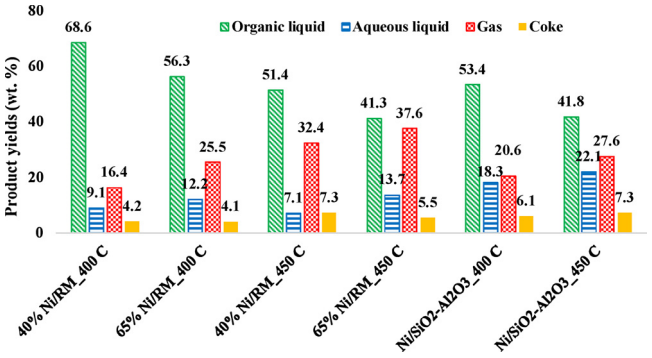

Fig. 9. Products yield distribution using Ni/RM (40% and 65% Ni loading) and commercial Ni/SiO2-Al2O3 catalysts at reaction temperatures of 400 °C and 450 °C.

Table 8
H_2 consumption, physicochemical properties of the liquid products, and gas product composition using commercial Ni/SiO2-Al2O3 catalyst.

Properties	Reaction time was 30 min					
	40%Ni/RM 400 °C	65%Ni/RM 400 °C	40%Ni/RM 450 °C	65%Ni/RM 450 °C	Ni/SiO_2-Al_2O_3 400 °C	Ni/SiO_2-Al_2O_3 450 °C
H_2 consumption (mol/g bio-oil)	0.053	0.072	0.056	0.083	0.061	0.095
Aqueous phase						
Water content (wt.%)	99.45	99.95	99.15	99.40	99.35	99.55
pH	6.91	6.93	6.94	6.96	6.87	6.89
HDO oil (organic phase)						
Elemental analysis (wt.%)						
N	0.31	0.30	0.26	0.17	0.21	0.13
C	82.52	83.11	83.13	83.18	79.81	82.94
H	15.82	16.59	16.61	16.65	11.65	15.66
O	1.35	0	0	0	8.33	1.27
HHV (MJ/kg)	45.77	45.81	45.83	45.85	42.58	45.16
pH	NA	NA	NA	NA	NA	NA
Water content (wt.%)	< DL	< DL	< DL	< DL	< DL	< DL
Density (g/ml)	0.79	0.78	0.78	0.78	0.91	0.81
Dynamic viscosity (cP)	1.37	1.31	1.30	1.30	3.43	1.38
Gas composition (mole %)						
CO	3.32	2.23	3.11	2.05	0	0
CO_2	5.52	4.19	4.25	3.17	4.12	0
CH_4	67.34	69.76	68.56	71.34	78.34	90.61
C_2H_4	8.26	8.66	8.47	9.14	7.34	4.23
C_3H_8	7.56	7.67	7.71	7.83	5.24	2.14
C_4H_{10}	5.45	5.28	5.33	4.15	3.14	1.87
C_5H_{12}	2.47	2.19	2.31	1.85	1.34	0.76

and coke formation compared to commercial Ni/SiO_2-Al_2O_3. After regeneration by burning off the coke and reducing with hydrogen, the activity of the Ni/RM catalyst was completely restored; in contrast the commercial catalyst that was not regenerable. This study showed that RM can serve as a promising nickel catalyst support for HDO process.

As an effective HDO catalyst, it will be required to address the performance of Ni/RM in a continuous packed-bed reactor configuration to replace the batch reactor for upgrading of bio-oil and evaluate the catalyst life. Additionally, cross-interactions of HDO intermediates on Ni/RM catalyst needs to be studied in future to get better understanding of the reaction mechanisms. Furthermore, detailed feasibility studies including technoeconomic analysis and energy balance for the entire pyrolysis-HDO process has to be carried out prior to scaling up of this process.

Acknowledgments

This research was supported by National Science Foundation under contract # 1445735 and Utah Science Technology and Research (USTAR). We would also thank Garret Smith, Kyle Christian and Brandon Sargent for supplying the bio oil. We would gratefully acknowledge Microscopy Core Facility at Utah State University.

Appendix A. Supplementary data

Supplementary material related to this article can be found, in the online version, at doi:https://doi.org/10.1016/j.apcatb.2018.05.008.

References

[1] S.H. Mohr, J. Wang, G. Ellem, J. Ward, D. Giurco, Projection of world fossil fuels by country, Fuel 141 (2015) 120–135.
[2] N.R. Singh, W.N. Delgass, F.H. Ribeiro, R. Agrawal, Estimation of liquid fuel yields from biomass, Environ. Sci. Technol. 44 (2010) 5298–5305.
[3] M. Patel, A. Kumar, Production of renewable diesel through the hydroprocessing of lignocellulosic biomass-derived bio-oil: a review, Renew. Sustain. Energy Rev. 58 (2016) 1293–1307.
[4] B. Ma, F.A. Agblevor, Polarity-based separation and chemical characterization of fast pyrolysis bio-oil from poultry litter, Biomass Bioenergy 64 (2014) 337–347.
[5] Y. Elkasabi, Q. Liu, Y.S. Choi, G. Strahan, A.A. Boateng, J.R. Regalbuto, Bio-oil hydrodeoxygenation catalysts produced using strong electrostatic adsorption q, Fuel 207 (2017) 510–521.
[6] Y. Luo, V.K. Guda, E.B. Hassan, P.H. Steele, B. Mitchell, F. Yu, Hydrodeoxygenation of oxidized distilled bio-oil for the production of gasoline fuel type, Energy Convers. Manag. 112 (2016) 319–327.
[7] Q. Li, P.H. Steele, F. Yu, B. Mitchell, E.M. Hassan, Pyrolytic spray increases levoglucosan production during fast pyrolysis, J. Anal. Appl. Pyrolysis 100 (2013) 33–40.
[8] S. Cheng, L. Wei, X. Zhao, Y. Huang, D. Raynie, C. Qiu, J. Kiratu, Y. Yu, Directly catalytic upgrading bio-oil vapor produced by prairie cordgrass pyrolysis over Ni/HZSM-5 using a two stage reactor, AIMS Energy 3 (2015) 227–240.
[9] Y. Luo, E.B. Hassan, V. Guda, R. Wijayapala, P.H. Steele, Upgrading of syngas hydrotreated fractionated oxidized bio-oil to transportation grade hydrocarbons, Energy Convers. Manag. 115 (2016) 159–166.
[10] M.B. Shemfe, S. Gu, P. Ranganathan, Techno-economic performance analysis of biofuel production and miniature electric power generation from biomass fast pyrolysis and bio-oil upgrading, Fuel 143 (2015) 361–372.
[11] L. Liu, Y. Liu, X. Gao, R. Zhang, Y. Zhai, Hydrodeoxygenation of bio-oil model

compounds over amorphous NiB/SiO2-Al2O3 catalyst in oil-water biphasic system, J. Fuel Chem. Technol. 45 (2017) 932–938.
[12] H. Jahromi, F.A. Agblevor, Upgrading of pinyon-juniper catalytic pyrolysis oil via hydrodeoxygenation, Energy 141 (2017) 2186–2195.
[13] X. Zhang, T. Wang, L. Ma, Q. Zhang, T. Jiang, Hydrotreatment of bio-oil over Ni-based catalyst, Bioresour. Technol. 127 (2013) 306–311.
[14] Y. Li, C. Zhang, Y. Liu, S. Tang, G. Chen, R. Zhang, X. Tang, Coke formation on the surface of Ni/HZSM-5 and Ni-Cu/HZSM-5 catalysts during bio-oil hydrodeoxygenation, Fuel 189 (2017) 23–31.
[15] X. Zhao, L. Wei, S. Cheng, J. Julson, Review of heterogeneous catalysts for catalytically upgrading vegetable oils into hydrocarbon biofuels, Catalysts 7 (2017) 83.
[16] S. Cheng, L. Wei, X. Zhao, J. Julson, Application, deactivation, and regeneration of heterogeneous catalysts in bio-oil upgrading, Catalysts 6 (2016) 195.
[17] J. Wildschut, F.H. Mahfud, R.H. Venderbosch, H.J. Heeres, Hydrotreatment of fast pyrolysis oil using heterogeneous noble-metal catalysts, Ind. Eng. Chem. Res. 48 (2009) 10324–10334.
[18] Y. Huang, L. Wei, X. Zhao, S. Cheng, J. Julson, Y. Cao, Z. Gu, Upgrading pine sawdust pyrolysis oil to green biofuels by HDO over zinc-assisted Pd/C catalyst, Energy Convers. Manag. 115 (2016) 8–16.
[19] S. Cheng, L. Wei, X. Zhao, E. Kadis, Y. Cao, J. Julson, Z. Gu, Hydrodeoxygenation of prairie cordgrass bio-oil over Ni based activated carbon synergistic catalysts combined with different metals, N. Biotechnol. 33 (2016) 440–448.
[20] V.A. Yakovlev, S.A. Khromova, O.V. Sherstyuk, V.O. Dundich, D.Y. Ermakov, V.M. Novopashina, M.Y. Lebedev, O. Bulavchenko, V.N. Parmon, Development of new catalytic systems for upgraded bio-fuels production from bio-crude-oil and biodiesel, Catal. Today 144 (2009) 362–366.
[21] E. Furimsky, Catalytic hydrodeoxygenation, Appl. Catal. A: Gen. 199 (2000) 147–190.
[22] A. Agrawal, K.K. Sahu, B.D. Pandey, Solid waste management in non-ferrous industries in India, Resour. Conserv. Recycl. 42 (2004) 99–120.
[23] S. Sushil, V.S. Batra, Catalytic applications of red mud, an aluminium industry waste: a review, Appl. Catal. B: Environ. 81 (2008) 64–77.
[24] B.K. Yathavan, F.A. Agblevor, Catalytic pyrolysis of pinyon-juniper using red mud and HZSM-5, Energy Fuels 27 (2013) 6858–6865.
[25] X. Lim, A. Sanna, J.M. Andresen, Influence of red mud impregnation on the pyrolysis of oil palm biomass-EFB, Fuel 119 (2014) 259–265.
[26] B. Klopries, W. Hodek, F. Bandermann, Catalytic hydroliquefaction of biomass with red mud and CO-MO_3 catalysts, Fuel 69 (1990) 448–455.
[27] C.K. Pratt, V. Christoverson, Hydrogenation of a model hydrogen-donor system using activated red mud catalyst, Fuel 61 (1982) 460–462.
[28] A. Eamsiri, W.R. Jackson, K.C. Pratt, V. Christoverson, M. Marshall, Activated red mud as a catalyst for the hydrogenation of coals and of aromatic compounds, Fuel 71 (1992) 449–453.
[29] J.J. Llano, R. Rosal, H. Sastre, F.V. Diez, Catalytic hydrogenation of anthracene oil with red mud, Fuel 73 (1994) 688–694.
[30] S. Ordóñez, H. Sastre, F.V. Díez, Characterisation and deactivation studies of sulfided red mud used as catalyst for the hydrodechlorination of tetrachloroethylene, Appl. Catal. B: Environ. 29 (2001) 263–273.
[31] J. Alvarez, R. Rosal, H. Sastre, F.V. Diez, Characterization and deactivation of sulfided red mud used as hydrogenation catalyst, Appl. Catal. A: Gen. 128 (1995) 259–273.
[32] S. Ordóez, H. Sastre, F.V. Díez, Catalytic hydrodechlorination of tetrachloroethylene over red mud, J. Hazard. Mater. 81 (2001) 103–114.
[33] M. Martino, R. Rosal, H. Sastre, F.V. Diez, Hydrodechlorination of dichloromethane, trichloroethane, trichloroethylene and tetrachloroethylene over a sulfided Ni/Mo-γ-alumina catalyst, Appl. Catal. B: Environ. 20 (1999) 301–307.
[34] L.C.A. De Oliveira, A.P. Heitmann, L.D. Almeida, S. Herman, A.A. Mansur, C.S. De Castro, U.F. De Alfenas, PET-modified red mud as catalysts for oxidative desulfurization reactions, J. Environ. Sci. 57 (2015) 3–5.
[35] J.R. Paredes, S. Ordóñez, A. Vega, Catalytic combustion of methane over red mud-based catalysts, Appl. Catal. 47 (2004) 37–45.
[36] S. Djerad, M. Crocoll, S. Kureti, L. Tifouti, W. Weisweiler, Effect of oxygen concentration on the NOx reduction with ammonia over V2O5–WO3/TiO2 catalyst, Catal. Today 113 (2006) 208–214.
[37] J. Yanik, A. Uddin, K. Ikeuchi, Y. Sakata, The catalytic effect of red mud on the degradation of poly(vinyl chloride) containing polymer mixture into fuel oil, Polym. Degrad. Stab. 73 (2001) 335–346.
[38] A. Sınag, M. Sungur, M. Canel, Effect of experimental conditions on the yields during the copyrolysis of mustafa kemal pasa (MKP) lignite (Turkey) with low-density polyethylene, Energy Fuels 20 (2006) 1609–1613.
[39] A.I. Cakici, J. Yanik, S. Uçar, T. Karayildirim, H. Anil, Utilization of red mud as catalyst in conversion of waste oil and waste plastics to fuel, J. Mater. Cycles Waste Manag. 6 (2004) 20–26.
[40] A. Iannibello, S. Marengo, A. Girelli, Bauxite-based catalysts in heavy crude oil hydrotreating, Appl. Catal. 3 (1982) 261–272.
[41] S. Uemiya, M. Uchida, H. Moritomi, R. Yoshiie, M. Nishimura, Ammonia decomposition catalyst with resistance to coexisting sulfur compounds, Mater. Trans. 46 (2005) 2709–2712.
[42] S.H. Khezri, N. Azimi, M. Mohammed-vali, B. Eftekhari-sis, Red mud catalyzed one-pot synthesis of nitriles from aldehydes and hydroxylamine hydrochloride under microwave irradiation, Arkivoc 15 (2007) 162–170.
[43] N.I. Bento, P.S.C. Santos, T.E. de Souza, L.C.A. Oliveira, C.S. Castro, Composites based on PET and red mud residues as catalyst for organic removal from water, J. Hazard. Mater. 314 (2016) 304–311.
[44] J. Li, L. Xu, P. Sun, P. Zhai, X. Chen, H. Zhang, Z. Zhang, W. Zhu, Novel application of red mud: facile hydrothermal-thermal conversion synthesis of hierarchical porous AlOOH and Al2O3 microspheres as adsorbents for dye removal, Chem. Eng. J. 321 (2017) 622–634.
[45] M. Senthil, K. Visagavel, C.G. Saravanan, K. Rajendran, Investigations of red mud as a catalyst in Mahua oil biodiesel production and its engine performance, Fuel Process. Technol. 149 (2016) 7–14.
[46] J. Ye, A. Hu, G. Ren, T. Zhou, G. Zhang, S. Zhou, Red mud enhances methanogenesis with the simultaneous improvement of hydrolysis-acidification and electrical conductivity, Bioresour. Technol. 247 (2018) 131–137.
[47] H. Jahromi, F.A. Agblevor, Hydrotreating of guaiacol: a comparative study of red mud-supported nickel and commercial Ni/SiO_2-Al_2O_3catalysts, Appl. Catal. A: Gen. 558 (2018) 109–121.
[48] R.F. Miller, J.D. Bates, T.J. Svejcar, F.B. Pierson, L.E. Eddleman, Technical Bulletin 152; Corvallis Agricultural Experiment Station, Oregon State University, Corvallis, OR, 2005.
[49] P.E. Carrara, T.R. Carroll, The determination of erosion rates from exposed tree roots in the Piceance basin, Colorado, Earth Surf. Process. 4 (1979) 307–317.
[50] R.J. Ansley, H.T. Wiedemann, M.J. Castellano, J.E. Slosser, Herbaceous restoration of juniper dominated grasslands with chaining and fire, Rangel. Ecol. Manage. 59 (2006) 171–178.
[51] C. Baughman, T.A. Forbis, L. Provencher, Response of two sagebrush sites to low-disturbance, mechanical removal of pinyon and juniper, Invasive Plant Sci. Manage. 3 (2010) 122–129.
[52] O.D. Mante, F.A. Agblevor, Catalytic pyrolysis for the production of refinery-ready biocrude oils from six different biomass resources, Green Chem. 16 (2014) 3364–3377.
[53] Z. Xinghua, W. Tiejun, M. Longlong, W. Chuangzhi, Aqueous-phase catalytic process for production of pentane from furfural over nickel-based catalysts, Fuel 89 (2010) 2697–2702.
[54] X. Zhang, L. Chen, W. Kong, T. Wang, Q. Zhang, J. Long, Y. Xu, L. Ma, Upgrading of bio-oil to boiler fuel by catalytic hydrotreatment and esterification in an efficient process, Energy 84 (2015) 83–90.
[55] R. Gavlak, R. Horneck, R.O. Miller, J. Kotuby-Amacher, Soil, Plant and Water Reference Methods for the Western Region, 3rd ed., (2005) 1679–169.
[56] S.V. Vassilev, D. Baxter, L.K. Andersen, C.G. Vassileva, An overview of the chemical composition of biomass, Fuel 89 (2010) 913–933.
[57] S. Chenna, R. Banerjee, P.A. Crozier, Atomic-scale observation of the Ni activation process for partial oxidation of methane using in situ environmental TEM, ChemCatChem 3 (2011) 1051–1059.
[58] Q. Jeangros, T.W. Hansen, J.B. Wagner, C.D. Damsgaard, R.E. Dunin-Borkowski, C. Hébert, J. Van Herle, A. Hessler-Wyser, Reduction of nickel oxide particles by hydrogen studied in an environmental TEM, J. Mater. Sci. 48 (2013) 2893–2907.
[59] I. Coronado, M. Stekrova, L. García Moreno, M. Reinikainen, P. Simell, R. Karinen, J. Lehtonen, Aqueous-phase reforming of methanol over nickel-based catalysts for hydrogen production, Biomass Bioenergy 106 (2017) 29–37.
[60] J. Pu, K. Nishikado, N. Wang, T.T. Nguyen, T. Maki, E.W. Qian, Core-shell nickel catalysts for the steam reforming of acetic acid, Appl. Catal. B: Environ. 224 (2017) 69–79.
[61] C. Boscagli, C. Yang, A. Welle, W. Wang, S. Behrens, K. Raffelt, J.D. Grunwaldt, Effect of pyrolysis oil components on the activity and selectivity of nickel-based catalysts during hydrotreatment, Appl. Catal. A: Gen. 544 (2017) 161–172.
[62] H.D. Demsash, K.V.K. Kondamudi, S. Upadhyayula, R. Mohan, Ruthenium doped nickel-alumina-ceria catalyst in glycerol steam reforming, Fuel Process. Technol. 169 (2018) 150–156.
[63] R. Molina, G. Poncelet, α-Alumina-supported nickel catalysts prepared from nickel acetylacetonate: a TPR study, J. Catal. 173 (1998) 257–267.
[64] D. Wierzbicki, R. Baran, R. Debek, M. Motak, T. Grzybek, M.E. Galvez, P. Da Costa, The influence of nickel content on the performance of hydrotalcite-derived catalysts in CO2 methanation reaction, Int. J. Hydrogen Energy 42 (2017) 23548–23555.
[65] H.-F. Wang, X.-Q. Gong, Y.-L. Guo, Y.-L. Guo, G.Z. Lu, P. Hu, A model to understand the oxygen vacancy formation in Zr-doped CeO_2: electrostatic interaction and structural relaxation, J. Phys. Chem. C 113 (2009) 10229–10232.
[66] V. Shapovalov, H. Metiu, Catalysis by doped oxides: CO oxidation by $Au_xCe_{1-x}O_2$, J. Catal. 245 (2007) 205–214.
[67] B. Li, H. Metiu, DFT studies of oxygen vacancies on undoped and doped La_2O_3 surfaces, J. Phys. Chem. C 114 (2010) 12234–12244.
[68] H.Y. Kim, H.M. Lee, R.G.S. Pala, V. Shapovalov, H. Metiu, CO oxidation by rutile TiO2 (110) doped with V, W, Cr, Mo, and Mn, J. Phys. Chem. C 112 (2008) 12398–12408.
[69] V.O.O. Gonçalves, P.M. de Souza, T. Cabioc'h, V.T. da Silva, F.B. Noronha, F. Richard, Hydrodeoxygenation of m-cresol over nickel and nickel phosphide based catalysts. Influence of the nature of the active phase and the support, Appl. Catal. B: Environ. 219 (2017) 619–628.
[70] S. Kadarwati, S. Oudenhoven, M. Schagen, X. Hu, M. Garcia-Perez, S. Kersten, C.Z. Li, R. Westerhof, Polymerization and cracking during the hydrotreatment of bio-oil and heavy fractions obtained by fractional condensation using Ru/C and NiMo/Al2O3 catalyst, J. Anal. Appl. Pyrolysis 118 (2016) 136–143.
[71] F.A. Agblevor, D.C. Elliott, D.M. Santosa, M.V. Olarte, S.D. Burton, M. Swita, S.H. Beis, K. Christian, B. Sargent, Red mud catalytic pyrolysis of pinyon juniper and single-stage hydrotreatment of oils, Energy Fuels 30 (2016) 7947–7958.
[72] S.K. Tanneru, P.H. Steele, Direct hydrocracking of oxidized bio-oil to hydrocarbons, Fuel 154 (2015) 268–274.
[73] T.S. Kim, S. Oh, J.Y. Kim, I.G. Choi, J.W. Choi, Study on the hydrodeoxygenative upgrading of crude bio-oil produced from woody biomass by fast pyrolysis, Energy 68 (2014) 437–443.
[74] H. Habazaki, M. Yamasaki, B.-P. Zhang, A. Kawashima, S. Kohno, T. Takai, K. Hashimoto, Co-methanation of carbon monoxide and carbon dioxide on

supported nickel and cobalt catalysts prepared from amorphous alloys, Appl. Catal. A: Gen. 172 (1998) 131–140.
[75] W. Wang, W. Chu, N. Wang, W. Yang, C. Jiang, Mesoporous nickel catalyst supported on multi-walled carbon nanotubes for carbon dioxide methanation, Int. J. Hydrogen Energy 41 (2016) 967–975.
[76] B. Nematollahi, M. Rezaei, E.N. Lay, Selective methanation of carbon monoxide in hydrogen rich stream over Ni/CeO2 nanocatalysts, J. Rare Earths 33 (2015) 619–628.
[77] O.D. Mante, F.A. Agblevor, S.T. Oyama, R. McClung, The effect of hydrothermal treatment of FCC catalysts and ZSM-5 additives in catalytic conversion of biomass, Appl. Catal. A: Gen. 445–446 (2012) 312–320.
[78] G.D. Strahan, C.A. Mullen, A.A. Boateng, Characterizing biomass fast pyrolysis oils by 13C NMR and chemometric analysis, Energy Fuels 25 (2011) 5452–5461.